

## **Supporting Information**

### **A pH sensitive Laser-Induced Fluorescence technique to monitor mass transfer in multiphase flows in microfluidic devices**

*Simon Kuhn and Klavs F. Jensen\**

## CFD modeling using OpenFOAM

In addition to the experimental comparison we also performed a numerical simulation of the Y-shaped mixing section using the open-source software OpenFOAM<sup>®</sup>. To address the passive mixing case we added a scalar equation to the already available incompressible *icoFoam* solver, which then solved the continuity equation

$$\frac{\partial u_i}{\partial x_i} = 0, \quad (1)$$

where  $u_i$  is the velocity in the  $i$  direction, the momentum equation,

$$\frac{\partial u_i}{\partial t} + u_j \frac{\partial u_i}{\partial x_j} = -\frac{1}{\rho} \frac{\partial p}{\partial x_j} + \nu \frac{\partial^2 u_i}{\partial x_j \partial x_j}, \quad (2)$$

where  $p$  is the pressure and  $\rho$  is the density, and the convection-diffusion equation for the concentration,  $c$ ,

$$\frac{\partial c}{\partial t} + u_j \frac{\partial c}{\partial x_j} = D \frac{\partial^2 c}{\partial x_j \partial x_j}. \quad (3)$$

To model the reactive mixing case, we modified the *icoFoam* solver further by adding three equations for the scalar species  $c_i$  undergoing the following reaction scheme,  $A + B \rightarrow C$ , by taking into account the reaction rate  $R$ ,<sup>1</sup>

$$\frac{\partial c_i}{\partial t} + u_j \frac{\partial c_i}{\partial x_j} = D \frac{\partial^2 c_i}{\partial x_j \partial x_j} + R. \quad (4)$$

The obtained concentration profiles at the two positions downstream of the mixing zone at  $x/d_H=4$  and  $x/d_H=40$  exhibit a good agreement with the measurements for the passive (Figure S1) and reactive (Figure S2) mixing case. Thus the accuracy of the pH-LIF technique is also supported by the numerical simulations.

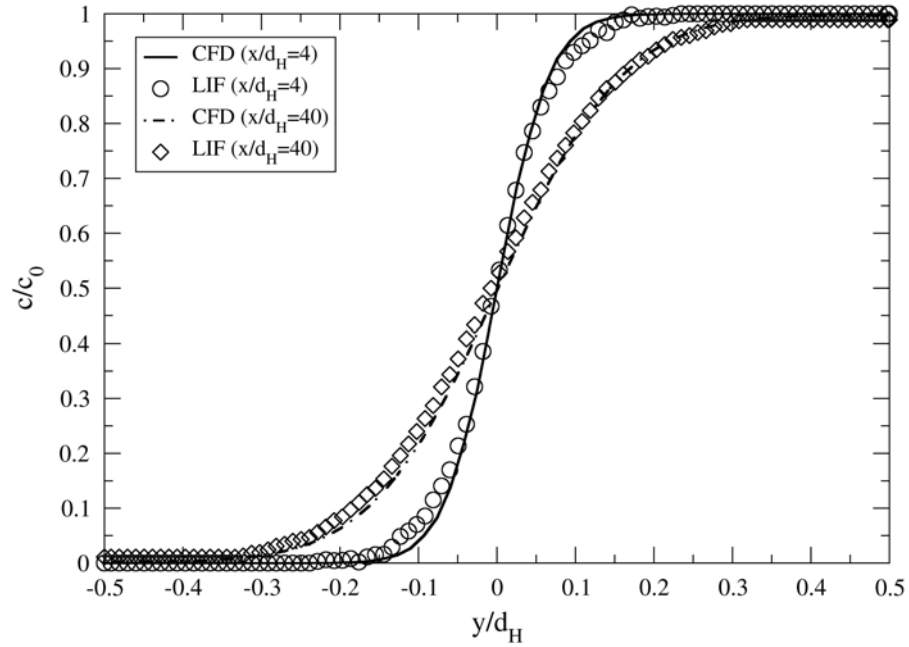


Figure S1: Comparison of concentration profiles obtained by LIF and CFD for the passive mixing case at positions  $x/d_H=4$  and  $x/d_H=40$  downstream of the mixing zone.

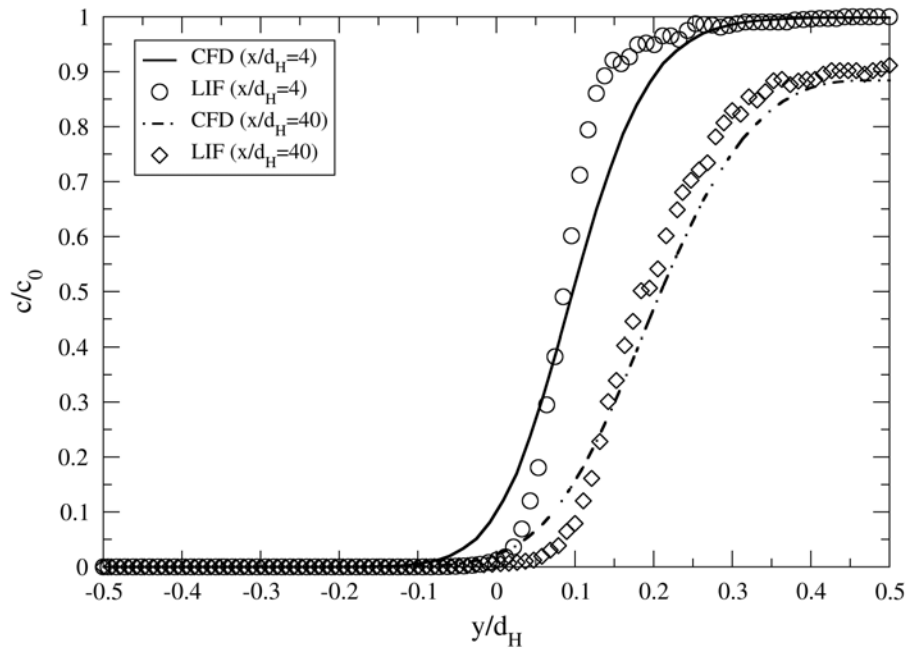


Figure S2: Comparison of concentration profiles obtained by LIF and CFD for the reactive mixing case at positions  $x/d_H=4$  and  $x/d_H=40$  downstream of the mixing zone.

## Two-phase flow distribution depending on the volume transport fraction $\dot{\epsilon}_G$

To further investigate the dependence of the observed  $k_L a$  value on the volume transport fraction (Figure 11) we took photographs of the entire microreactor to visualize the two-phase flow distribution. Below a certain gas phase transport fraction Taylor flow is no longer established as a constant train of bubbles. This is visualized in Figure S3, the left hand side shows a volume transport fraction of  $\dot{\epsilon}_G = 0.4$ , the right hand side of  $\dot{\epsilon}_G = 0.8$ . For low gas fractions, individual bubbles enter the reactor (right hand side of the left image), which then regroup throughout the microchannel. This regrouping leads to “clusters” of bubbles moving through the reactor, which drastically reduces the intensity of the secondary flow structures in the continuous phase, which directly affects mass transfer as well. For higher gas fractions instead, stable Taylor flow is established and the observed secondary flow motions drive the mass transfer. We observed this transition to stable Taylor flow take place at volume transport fractions above  $\dot{\epsilon}_G = 0.6$ .

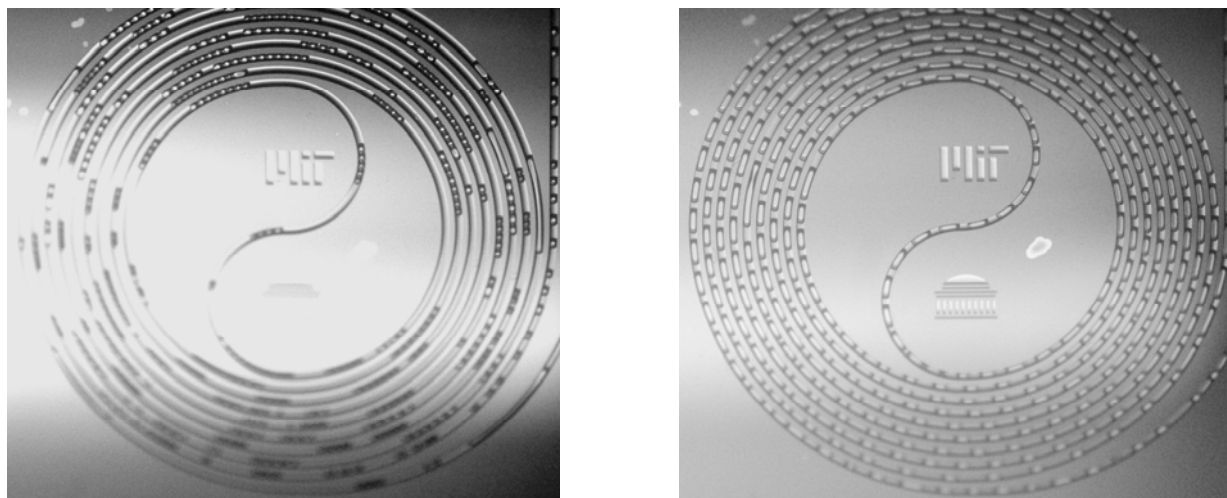


Figure S3: Photographs of the two-phase flow distribution depending on the volume transport fraction. Left:  $\dot{\epsilon}_G = 0.4$ . Right:  $\dot{\epsilon}_G = 0.8$ .

## References

- (1) Baldyga, J.; Bourne, J. R.; Walker, B., Non-isothermal micromixing in turbulent liquids: Theory and experiment. *The Canadian Journal of Chemical Engineering* **1998**, 76, (3), 641-649.